



Libration driven elliptical instability

David Cébron, Michael Le Bars, J. Noir, J. M. Aurnou

► To cite this version:

David Cébron, Michael Le Bars, J. Noir, J. M. Aurnou. Libration driven elliptical instability. *Physics of Fluids*, 2012, 24 (6), pp.061703. 10.1063/1.4729296 . hal-00708997

HAL Id: hal-00708997

<https://hal.science/hal-00708997>

Submitted on 16 Jun 2012

HAL is a multi-disciplinary open access archive for the deposit and dissemination of scientific research documents, whether they are published or not. The documents may come from teaching and research institutions in France or abroad, or from public or private research centers.

L'archive ouverte pluridisciplinaire **HAL**, est destinée au dépôt et à la diffusion de documents scientifiques de niveau recherche, publiés ou non, émanant des établissements d'enseignement et de recherche français ou étrangers, des laboratoires publics ou privés.

Libration driven elliptical instability

D. Cébron^{1,2,*}, M. Le Bars¹, J. Noir^{2,3}, and J.M. Aurnou³

¹ *CNRS and Aix-Marseille Univ., IRPHE (UMR 7342), 13384, Marseille cedex 13, France.*

² *Institut für Geophysik, ETH Zürich, Sonneggstrasse 5, Zürich, CH-8092, Switzerland.*

³ *Department of Earth and Space Sciences, University of California, Los Angeles, CA 90095-1567 USA.*

(Dated: June 17, 2012)

The elliptical instability is a generic instability which takes place in any rotating flow whose streamlines are elliptically deformed. Up to now, it has been widely studied in the case of a constant, non-zero differential rotation between the fluid and the elliptical distortion with applications in turbulence, aeronautics, planetology and astrophysics. In this letter, we extend previous analytical studies and report the first numerical and experimental evidence that elliptical instability can also be driven by libration, i.e. periodic oscillations of the differential rotation between the fluid and the elliptical distortion, with a zero mean value. Our results suggest that intermittent, space-filling turbulence due to this instability can exist in the liquid cores and sub-surface oceans of so-called synchronized planets and moons.

PACS numbers: 47.32.Ef, 95.30.Lz, 47.20.Cq

The longitudinal libration of a so-called synchronized planet or moon, i.e. the oscillation of its axial rotation rate whose mean value is otherwise equal to the orbital rotation rate, arises through its gravitational coupling with its closest neighbors [1, 2]. In the body interior, the interaction of a fluid layer (e.g. an iron rich liquid core or a subsurface ocean) with the surrounding librating solid shell resulting from viscous, topographic, gravitational or electromagnetic coupling, leads to energy dissipation and angular momentum transfer that need to be accounted for in the planet thermal history and orbital dynamics, and possibly in its magnetic state [3]. A number of studies has been devoted to libration-driven flows in axisymmetric containers in order to investigate the role of the viscous coupling. It has been shown that longitudinal libration in an axisymmetric container can drive inertial waves in the bulk of the fluid as well as boundary layer centrifugal instabilities in the form of Taylor-Görtler rolls [4–9]. In addition, laboratory and numerical studies [9–12] have corroborated the analytically predicted generation of a mainly retrograde axisymmetric and stationary zonal flow in the bulk, based upon non-linear interactions within the Ekman boundary layers [9–11, 13, 14]. Although practical to isolate the effect of viscous coupling, the spherical approximation of the core-mantle or ice shell-subsurface ocean boundaries, herein generically called the CMB, is not fully accurate from a planetary point of view and very restrictive from a fluid dynamics standpoint. Indeed, due to the rotation of the planet, the gravitational interactions with companion bodies and the low order spin-orbit resonance of the librating planets we are considering, the general figure of the CMB must be ellipsoidal with a polar flattening and a tidal bulge pointing on average toward the main gravitational partner [15].

The fluid dynamics that occurs in a rapidly rotating ellipsoidal cavity has been widely studied in the case of constant but different rotation rates of the fluid and the elliptical distortion. This corresponds in geophysical terms to a non-synchronized body with a constant spin rate Ω_0 , subject to dynamical tides rotating at the constant orbital rotation rate Ω_{orb} . In particular, it has been shown that this elliptically deformed base flow can be destabilized by the so-called tidally-driven elliptical instability or TDEI [16, 17].

Generally speaking, the elliptical instability can be seen as the inherent local instability of elliptical streamlines [18–20], or as the parametric resonance between two free inertial waves (resp. modes) of the rotating unbounded (resp. bounded) fluid and an elliptical strain, which is not an inertial wave or mode [21, 22]. Such a resonance mechanism, confirmed by numerous works in elliptically deformed cylinders [e.g. 23–25] and ellipsoids [26–28], also operates for triadic resonance of three inertial modes, proposed to explain the secondary instability of the elliptical instability [29, 30]. This triadic resonance of three inertial modes also applies for the inertial precessional instability in cylinders [31, 32] and spheroids [33, 34]: there, the base flow forced by precession is itself an inertial mode (e.g. the so-called Poincaré or tilt-over mode in the spheroid [35–38]), which resonates with two inertial modes.

It has been shown that selected resonances of the TDEI are sensitive to the ratio of the rotation rates of the fluid and the elliptical distortion [28, 39]. In particular, the elliptical instability is known to vanish in the case of synchronous rotation $\Omega_0 = \Omega_{orb}$. But theoretical arguments suggest that oscillations around this synchronous state may be sufficient to excite elliptical instability [17, 40, 41]. This could be of fundamental importance in planetary liquid cores and subsurface oceans of synchronized bodies, where librations are generically present. This letter thus

*Electronic address: david.cebron@erdw.ethz.ch

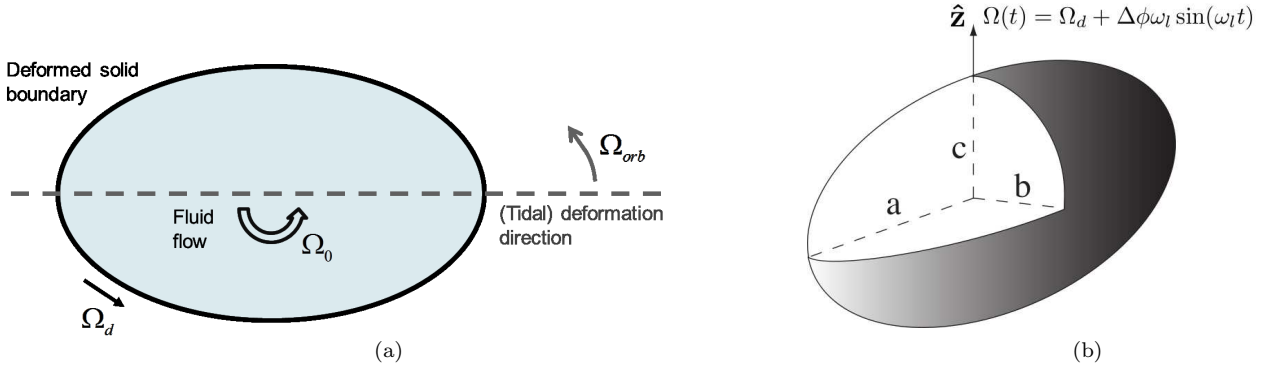


FIG. 1: (a) Mean rotation rates involved in our modeled planetary fluid layer: the elliptical (tidal) deformation rotates at the mean orbital rate Ω_{orb} , the external solid boundary has a constant tangential velocity imposed by the mean planetary spin rate Ω_d and the fluid mean rotation rate in the bulk of the fluid is Ω_0 (possibly different from Ω_d in a general case [12]). (b) Schematic view of the oscillating triaxial ellipsoidal container.

aims at validating the existence of a libration driven elliptical instability, hereafter referred to as LDEI. To do so, we first extend previous analytical studies [17, 40, 41] using a local WKB (Wentzel-Kramers-Brillouin) approach that allows us to determine a generic formula for the growth rate of LDEI. We then present the numerical and experimental validation of the existence of the LDEI, in good agreement with the theoretical results. Finally, implications for planets and moons are briefly discussed.

We consider a homogeneous, non-conductive, incompressible, newtonian fluid enclosed in a librating triaxial ellipsoid (fig.1). In the container frame of reference, the equation of the ellipsoidal boundary is written as $x^2/a^2 + y^2/b^2 + z^2/c^2 = 1$, where (x, y, z) is a cartesian coordinate system with its origin at the center of the ellipsoid, with $\hat{\mathbf{x}}$ along the long equatorial axis a , $\hat{\mathbf{y}}$ along the short equatorial axis b , and $\hat{\mathbf{z}}$ along the rotation axis c . We define the ellipticity $\beta = (a^2 - b^2)/(a^2 + b^2)$ and the aspect ratio $c^* = c/R$, where $R = \sqrt{(a^2 + b^2)/2}$ is the mean equatorial radius. The motion of longitudinal libration of the container is modeled by a time dependency of its axial rotation rate $\Omega(t) = \Omega_d + \Delta\phi\omega_l \sin(\omega_l t)$, where Ω_d is the mean rotation rate of the container (d for diurnal), $\Delta\phi$ the amplitude of libration in radians and ω_l the angular frequency of libration. In the frame of reference attached to the container, the equations of motion, made dimensionless using R as the length scale and Ω_d^{-1} as the time scale, become:

$$\frac{\partial \mathbf{u}}{\partial t} - \mathbf{u} \times (\nabla \times \mathbf{u}) + 2 [1 + \varepsilon \sin(ft)] \hat{\mathbf{z}} \times \mathbf{u} = -\nabla \Pi + E \nabla^2 \mathbf{u} - \varepsilon f \cos(ft) (\hat{\mathbf{z}} \times \mathbf{r}), \quad (1)$$

$$\nabla \cdot \mathbf{u} = 0. \quad (2)$$

In (1), Π is the reduced pressure, which includes the time-variable centrifugal acceleration. The Ekman number E is defined by $E = \nu/(\Omega_d R^2)$, where ν is the kinematic viscosity, the dimensionless libration frequency f is defined as $f = \omega_l/\Omega_d$, and ε is the libration forcing parameter defined by $\varepsilon = \Delta\phi f$. In the limit of small Ekman numbers, the flow can be decomposed into an inviscid component \mathbf{U} in the volume and a viscous boundary layer flow $\tilde{\mathbf{u}}$ that satisfies the no-slip boundary condition on the CMB. Introducing this separation, [40] proposed the following solution

to the inviscid equations of motion subject to the non-penetration condition at the CMB:

$$\mathbf{U} = -\varepsilon \sin(ft) [\hat{\mathbf{z}} \times \mathbf{r} - \beta \nabla(xy)]. \quad (3)$$

It can be shown that eq. (3) provides a solution of the inviscid form of (1) in the bulk; the inertial forces are balanced by the pressure gradient. No net zonal flow can result from the non-linear interactions in the quasi-inviscid interior [13], since pressure gradients alone cannot drive net zonal flows. However, the no-slip boundary condition is not entirely fulfilled by this solution: viscous corrections in the Ekman boundary layer must be considered, whose non-linear interactions generate a zonal flow in the bulk [10, 13, 14], as observed in axisymmetric containers [9–12].

In addition to these laminar and mostly two-dimensional (2D) motions, Kerswell and Malkus [40] first suggested that turbulent three-dimensional (3D) motions can be excited by an elliptical instability corresponding to a parametric resonance involving two free inertial waves of the rotating fluid and strain of the inviscid base flow (3), from which energy is extracted. Since the base flow is of azimuthal wavenumber $m = 2$ and temporal frequency f , this parametric resonance occurs only when $m_a - m_b = \pm m = \pm 2$ and $\lambda_a - \lambda_b = \pm f$, where m_a, m_b are the azimuthal wavenumbers of the two resonating free inertial waves and λ_a, λ_b are their frequencies non-dimensionalized by Ω_d . In addition to these resonance conditions, the two waves must have close radial and azimuthal structures to interact positively, corresponding to the so-called principal resonances [42]. This set of rules forms the basis for a global analysis of the elliptical instability, which thus requires an exact description of the inertial modes in the considered ellipsoidal geometry. Unfortunately, little is known about inertial modes for the finite values of β considered in the present study. This makes a complete characterization of the elliptical instability by global analysis presently out of reach for our simulations and experiments.

As an alternative, a local stability analysis of the base flow (3) can be performed, independently of the geometry of the container. Here, we make use of the results presented in [41] for the special case $f = 1$, later complemented [17]. The local analysis is based on the WKB method [20], which allows an upper bound to be derived for the growth rate of the elliptical instability. In this approach, perturbations are assumed to be sufficiently localized so as to be advected along flow trajectories. The perturbations are sought in the form of local plane waves characterized by their wavevector $\mathbf{k}(t)$, with norm $k \gg 1$, and tilted by an angle ζ to the rotation axis. Elliptical instability appears by resonance of two identical plane waves, only differing by their direction of propagation. The inviscid growth rate, σ_{inv} , can be determined by solving the Euler equations at the first order in the forcing amplitude $\beta\varepsilon$, yielding

$$\sigma_{inv} = \frac{16 + f_{res}^2}{64} \beta\varepsilon, \quad (4)$$

where $f_{res} \neq 0$ stands for a resonant forcing frequency [see details in ref. 17]. In the strict WBK limit $k \gg 1$, the dispersion relation between the forcing frequency and the excited plane waves is $f_{res}/2 = \pm 2 \cos \zeta$; hence, all forcing frequencies between -4 and $+4$ should be resonant. However, by accounting for the shape of the container and for viscous damping, similarly to the TDEI, resonances are only possible for selected couples of inertial waves, especially at the rather large Ekman numbers accessible to numerics [20, 28]. Thus, the system resonates only for selected values of the forcing frequency. Introducing a small detuning between the libration frequency f and a given exact resonance f_{res} [see method in ref. 20, for the standard case of TDEI] and taking into account the dominant viscous damping in the Ekman layer, it can be shown that excitation of the instability takes place around each resonant frequency in a band $f \in [f_{res} - \sigma_{inv}; f_{res} + \sigma_{inv}]$, where the typical growth rate is

$$\sigma = \sqrt{\sigma_{inv}^2 - (f_{res} - f)^2} - KE^{1/2}, \quad (5)$$

with $K \in [1; 10]$ a constant of order 1, which depends on the excited mode. The first term on the left hand side of (5) defines the range of unstable frequencies around a particular resonance; the second term describes the viscous damping of the instability. Besides the strict WBK limit, we expect this equation to be generally valid, once the specific values of the resonant frequency f_{res} and of the damping factor K have been determined [see validation for the case of TDEI in ref. 28]. Since both f_{res} and K depend on the selected inertial waves, both values can vary with the shape of the container.

To quantitatively validate the existence of LDEI and the above analytical results, we combine a systematic numerical study with selected laboratory experiments. We use the software Comsol Multiphysics® based on the finite elements method to perform our simulations. We work in the container frame of reference where the ellipsoidal shape of the container is stationary, and we solve the equations of motion (1) subject to no-slip boundary conditions, starting from a fluid at rest at time $t = 0$. We refer the reader to [43] for more informations on the numerical method. A first series of computations has been performed in 2D to test the realization of the inviscid base flow (3). A typical result is shown in figure 2. After a transient behavior scaling as a typical viscous time in $t \sim E^{-1}$ (figure 2a), the theoretical

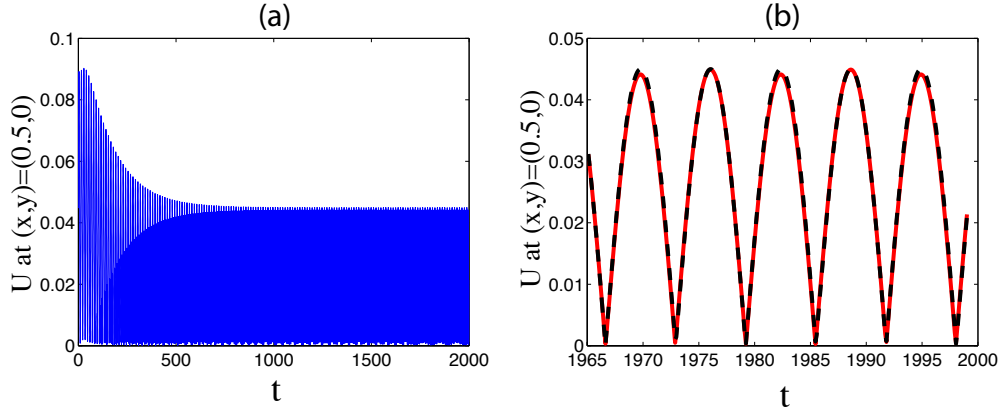


FIG. 2: (color online) (a) Temporal evolution of $U = |\mathbf{u}|$ at the location $(x = 0.5, y = 0)$, as calculated by the 2D version of our numerical model for $f = 0.5$, $\varepsilon = 0.1$, $\beta = 0.1$ and $E = 4 \times 10^{-4}$. (b) Zoom ($t > 1965$) of figure (a) once the flow is established: the continuous gray curve (red online) stands for the numerical results, and the dashed black curve for the theoretical flow (3).

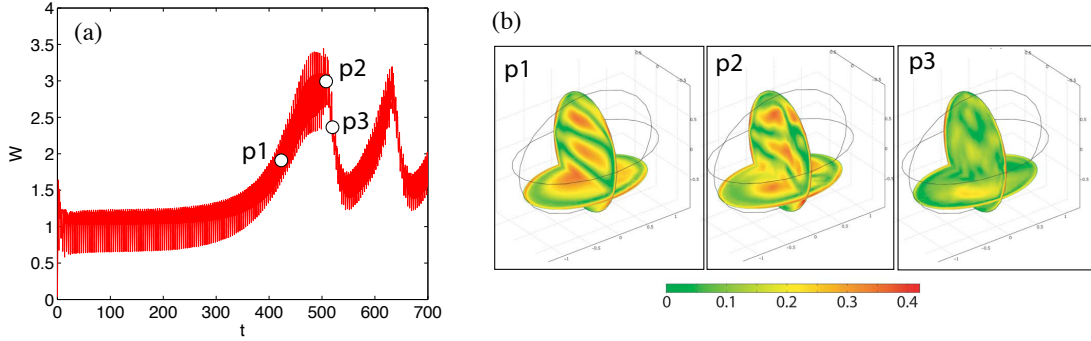


FIG. 3: (color online) (a) Time evolution of the absolute value of the axial velocity integrated over the whole container, non-dimensionalized by the mean value between times $t = 100$ and $t = 200$ (i.e. after the spin-up and before the potential destabilization). Numerical simulations are performed for $E = 5 \times 10^{-4}$, $\beta = 0.44$, $f = 1.76$, $\varepsilon = 0.92$ and $c^* = 0.95$. (b) $|\mathbf{u}|$, in a meridional cross section and in the plane $z = -0.5$. The sequence shows, from left to right, the typical field $|\mathbf{u}|$ during the exponential growth, at saturation and during the collapse.

base flow (3) is indeed established in the bulk (figure 2b), whereas the corrections necessary to fulfill the tangential part of the boundary conditions are restricted to the Ekman layer of depth $E^{-1/2}$. In the 3D ellipsoid, the Ekman pumping associated with the Ekman layer acts to significantly accelerate the establishment of the base flow, and we thus expect (3) to be the starting velocity field.

Series of numerical simulations have then been performed in a triaxial ellipsoid as a function of the libration frequency f , the libration amplitude ε and the aspect ratio c^* , keeping $E = 5 \times 10^{-4}$ and $\beta = 0.44$. An example of the temporal evolution of the absolute value of the axial velocity integrated over the volume, W , is presented in figure 3a for the case $f = 1.76$, $\varepsilon = 0.92$ and $c^* = 0.95$. Libration driven elliptical instability is present, characterized by intense 3D motions with rich temporal dynamics on typical times much longer than the spin and libration periods. In particular, we observe characteristic cycles of growth, saturation, collapses and relaminarization towards the base flow, already observed for the classical case of TDEI [28]. The typical changes in the flow field during one cycle are illustrated in figure 3b which shows the norm of the velocity in meridional and equatorial cross sections.

The growth rate of LDEI can be obtained by fitting the growing parts of time series of the integrated axial velocity W with an exponential function. The systematic evolution of this growth rate with f for $c^* = 1$ is shown in figure 4a, in comparison with the analytical formula (5), where f_{res} and K have been determined by adjusting (5) to each of the two local maxima of the numerically determined growth rate. We observe two bands of frequency centered around $f_{res} \sim 1.83$ and $f_{res} \sim 1.67$ where an elliptical instability grows. Good agreement is recovered for all neighboring values of f , validating the generic equation (5).

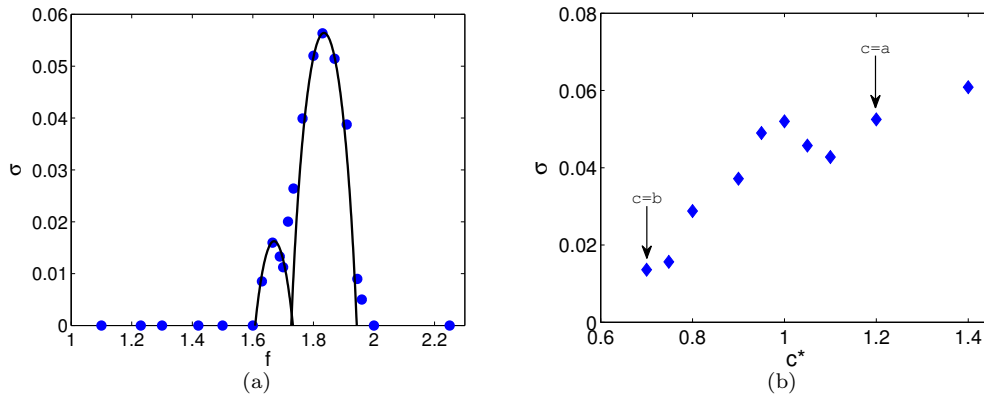


FIG. 4: (color online) Systematic numerical determination of the growth rate σ of the LDEI for $E = 5 \times 10^{-4}$, $\beta = 0.44$, $\varepsilon = 0.991$ (σ is set to 0 when the LDEI is not excited). (a) As a function of the libration frequency f for $c^* = 1$. Also shown here as a solid curve is the theoretical growth rate (5), where f_{res} and K have been determined by adjusting the analytical formula to each of the two local maxima of the numerical growth rate. (b) As a function of the aspect ratio c^* for $f = 1.8$. Note that the LDEI is excited in spheroidal geometries ($c = b$ or $c = a$).

The systematic evolution of the growth rate as a function of the aspect ratio c^* at a fixed resonant frequency $f = 1.8$ is shown in figure 4b. Although less dramatically than the frequency detuning, the geometrical factor c^* can also alter the growth rate of the elliptical instability at a given frequency. We observe that the optimal geometry at the resonant frequency $f = 1.83$ is realized for $c^* \sim 1$, as already shown in [43] for the classical elliptical instability (TDEI). In contrast with the TDEI studied in [43], we have no theoretical arguments that precludes the excitation of the LDEI in spheroidal geometries ($c = b$ or $c = a$). In figure 4b, we label these two particular cases, showing that the growth rates in these geometries are positive. Note that this does not refute the conclusions of [44], who show that libration in longitude cannot produce a direct resonance of an inertial mode. Here, the resonance does not occur directly between a mode and the forcing but between two modes and the forcing in a parametric coupling. The modes excited in the LDEI are not at the frequency of the forcing (which would be the case for a direct forcing), it is their frequency difference that is equal to f .

To further validate the existence of LDEI, we have also performed selected laboratory experiments (fig. 5). These allow us to reach smaller values of the Ekman number, and hence to access more chaotic flows, with the inconvenience being the difficulty in acquiring precise quantitative measurements and in changing the shape of the container. Except for the container, the laboratory apparatus is the same as in ref. [8] and [11]. It consists in an oscillating tank filled with water and centered on a turntable rotating at a constant angular velocity $\Omega_d = 0.5$ Hz. In order to perform quantitative measurements using Laser Doppler Velocimetry (LDV), the container consists in one hemispheroid CNC (Computer Numerical Control) machined from cast acrylic cylindrical blocks that is polished optically clear, with a top flat lid that avoids optical distortions. This geometry, corresponding to a “half-ellipsoidal” container, does not allow modes of the elliptical instability that are antisymmetric around the equator. Note also that because of manufacturing constraints, the small axis and the rotation axis of the container are equal, with $a = 127$ mm, $b = c = 89$ mm. The experimental parameters are then $\beta = 0.34$, $c^* = 0.812$ and $E = 2.7 \times 10^{-5}$; f and ε have been changed systematically to explore the ranges $f \in [0.5 - 2]$ with $\varepsilon = 1$, and $\varepsilon \in [0 - 1.6]$ with $f = 1$, respectively. Similar to the numerical experiments, we observe a resonance band, here $f \in [1.43 - 1.66]$, that is characterized by strong, intermittent, space-filling turbulence. These cases are marked by periods dominated by strong, small-scale, shear structures, followed by relaminarization period. These flows are not due to shear instabilities since the system does not exhibit any turbulence at higher frequency, for which the Rossby number is larger. Since no direct resonance can occur, if a shear instability were developing for a critical Rossby number it should remain unstable at larger forcing, regardless of the frequency.

An example of the measured azimuthal velocity is shown in figure 6 for $f = 1.46$. As mentioned earlier, the observed chaotic behavior of the flow as well as the fact that this behavior only appears for specific frequencies are characteristic of the elliptical instability. Assuming the existence of a resonant peak of LDEI at $f = 1.46$, the WKB approach (5) yields a typical growth time $1/(\sigma\Omega_d)$ of the instability ranging between 21s for a lower bound of the damping factor $K = 1$ and 37s for an upper bound of the damping factor $K = 10$. As shown in figure 6, these values are in good agreement with measurements during each growing phase of the azimuthal flow, further validating the interpretation of this chaotic behavior in terms of LDEI. Finally, note that even if no resonant cases have been obtained in this work

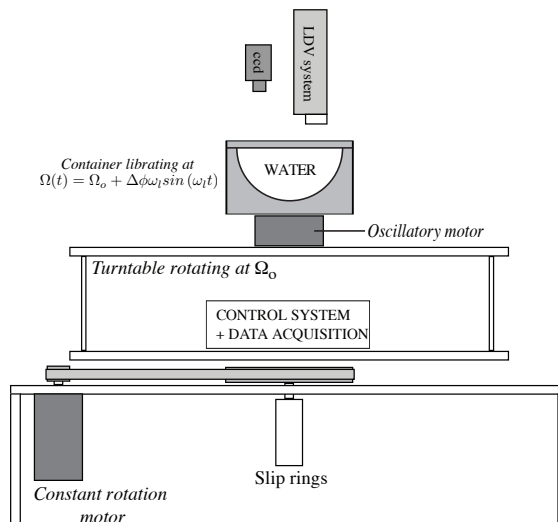


FIG. 5: Schematic view of the laboratory experiment and of the ultraLDV system [11], oriented to perform measurements of the azimuthal velocity. No LDV measurements of the azimuthal velocity can be readily performed in the case of an ellipsoidal container with a non-axisymmetric equatorial cross-section. Indeed, except if the LDV is moving with the tank, no relative position of the LDV with the container can be found such that the two laser beams remain coplanar over a libration cycle. A co-librating configuration is not achievable in the present experimental set-up due to the large centrifugal acceleration involved. Therefore, LDV measurements are performed with a "half-ellipsoidal" container, the northern half of the ellipsoid being replaced with a flat plate of acrylic.

with $f \leq 1$ [the relevant planetary range for f according to ref. 8], the WKB analysis predicts unambiguously that the LDEI can be excited for an arbitrary $|f| < 4$ provided that E is sufficiently small. Experiments at lower E should confirm it in the future. But the first experimental results presented here, in addition to the numerical simulations and in agreement with the theoretical analysis, already illustrate the generic feature of the libration driven elliptical instability, which appears for different geometries and various ranges of parameters.

In conclusion, studies of flows driven by longitudinal libration made using a spherical CMB approximation suggest that purely viscous coupling does not lead to significant planetary energy dissipation, angular momentum transfer nor magnetic field induction [9]. These conclusions should be re-addressed in accounting for the specific triaxial shape of the considered planets, since space-filling turbulence is observed in the present numerical and laboratory experiments in which LDEI is excited. A complete understanding of the elliptical instability excited by libration in celestial bodies requires the characterization of the inertial modes, their frequency and their viscous decay factor in the appropriate geometry and for the low values of the Ekman number relevant to planetary applications. Nevertheless, the relevance of a LDEI mechanism at planetary settings can be ascertained using the theoretical WKB approach presented here, by estimating a lower bound of the equatorial ellipticity leading to a positive growth rate σ . Using typical values for forced longitudinal libration [8] of $f = 1$, $E \sim 10^{-14}$, $\varepsilon \sim 10^{-4}$, a decay factor $K = 1$ and assuming a perfect resonance, equation (5) yields to a minimum equatorial ellipticity $\beta \sim 10^{-3}$ for excitation of LDEI. This first order estimate is qualitatively comparable with the values expected for Mercury, Europa or Io. Thus, the space-filling turbulence resulting from LDEI should exist within the fluid interiors of librating terrestrial bodies.

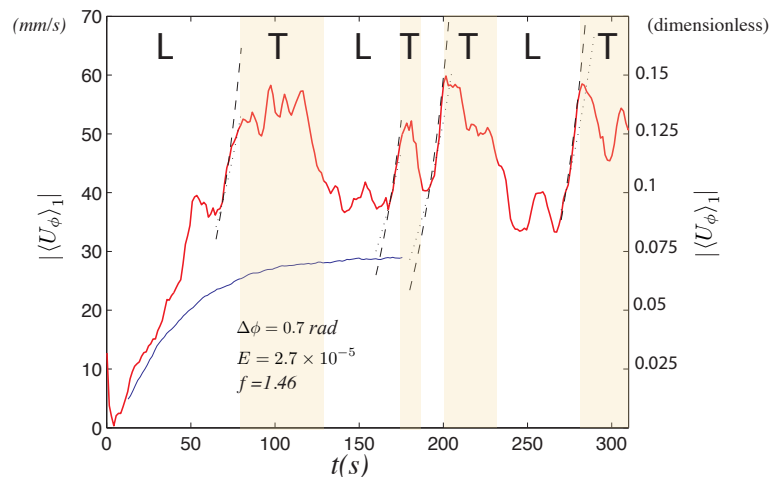


FIG. 6: (color online) Time evolution of the norm of the azimuthal velocity averaged over 10 oscillations for $\Delta\phi = 0.7$ rad ($\varepsilon \sim 1$) with $\beta = 0.34$ and $f = 1.46$ (continuous upper curve, red online); $\beta = 0.06$ and $f = 1.40$ (continuous upper curve, blue online). The measurements are performed at a cylindrical radius $S_z = 48$ mm along the short axis of the mean equatorial ellipse, 1 cm below the top flat surface. We perform a sliding window averaging over 10 oscillations with an overlap of 90%. In addition we represent the WKB exponential growth for two extreme values of the damping factor, $K = 1$ (dotted black) and $K = 10$ (dashed black). The letters L and T stand for Laminar and Turbulent. The periods of turbulence, as observed in direct visualizations, are qualitatively represented by the bands.

For this work, D. Cébron was partially supported by the ETH Zürich Postdoctoral fellowship Program as well as by the Marie Curie Actions for People COFUND Program.

-
- [1] C. F. Yoder, “Venus’ free obliquity,” *Icarus*, vol. 117, no. 2, pp. 250–286, 1995.
 - [2] R. L. Comstock and B. G. Bills, “A solar system survey of forced librations in longitude,” *Journal of Geophysical Research-Planets*, vol. 108, no. E9, pp. 1–13, 2003.
 - [3] M. Le Bars, M. Wiczkorek, Ö. Karatekin, D. Cébron, and M. Laneuville, “An impact-driven dynamo for the early moon,” *Nature*, vol. 479, pp. 215–218, 2011.
 - [4] K. D. Aldridge, *An Experimental Study of Axisymmetric Inertial Oscillations of a Rotating Liquid Sphere*. PhD thesis, Massachusetts Institute of Technology, 1967.
 - [5] K. D. Aldridge and A. Toomre, “Axisymmetric inertial oscillations of a fluid in a rotating spherical container,” *Journal of Fluid Mechanics*, vol. 37, pp. 307–323, 1969.
 - [6] K. D. Aldridge, “Inertial waves and Earth’s outer core,” *Geophysical Journal of the Royal Astronomical Society*, vol. 42, no. 2, pp. 337–345, 1975.
 - [7] A. Tilgner, “Driven inertial oscillations in spherical shells,” *Physical Review E*, vol. 59, no. 2, pp. 1789–1794, 1999.
 - [8] J. Noir, F. Hemmerlin, J. Wicht, S. Baca, and J. M. Aurnou, “An experimental and numerical study of librationally driven flow in planetary cores and subsurface oceans,” *Physics of the Earth and Planetary Interiors*, vol. 173, pp. 141–152, 2009.
 - [9] M. Calkins, J. Noir, J. Eldredge, and J. M. Aurnou, “Axisymmetric simulations of libration-driven fluid dynamics in a spherical shell geometry,” *Physics of Fluids*, vol. 22, pp. 1–12, 2010.
 - [10] C.-Y. Wang, “Cylindrical tank of fluid oscillating about a state of steady rotation,” *Journal of Fluid Mechanics*, vol. 41, pp. 581–592, 1970.
 - [11] J. Noir, M. Calkins, M. Lasbleis, J. Cantwell, and J. M. Aurnou, “Experimental study of libration-driven zonal flows in a straight cylinder,” *Physics of the Earth and Planetary Interiors*, vol. 182, pp. 98–1106, 2010.
 - [12] A. Sauret, D. Cébron, C. Morize, and M. Le Bars, “Experimental and numerical study of mean zonal flows generated by librations of a rotating spherical cavity,” *Journal of Fluid Mechanics*, vol. 662, pp. 260–268, 2010.
 - [13] F. Busse, “Mean zonal flows generated by librations of a rotating spherical cavity,” *Journal of Fluid Mechanics*, vol. 650, pp. 505–512, 2010.
 - [14] F. Busse, “Zonal flow induced by longitudinal librations of a rotating cylindrical cavity,” *Physica D: Nonlinear Phenomena*, vol. 240, pp. 208–211, 2011.
 - [15] P. M. Goldreich and J. L. Mitchell, “Elastic ice shells of synchronous moons: Implications for cracks on Europa and non-synchronous rotation of Titan,” *Icarus*, vol. 209, no. 2, pp. 631–638, 2010.
 - [16] R. R. Kerswell, “Elliptical instability,” *Annual Review of Fluid Mechanics*, vol. 34, pp. 83–113, 2002.

- [17] D. Cebron, M. Le Bars, C. Moutou, and P. Le Gal, "Elliptical instability in terrestrial planets and moons," *Astronomy and Astrophysics*, vol. 539, no. A78, 2012.
- [18] B. Bayly, "Three-dimensional instability of elliptical flow," *Physical review letters*, vol. 57, no. 17, pp. 2160–2163, 1986.
- [19] F. Waleffe, "On the three-dimensional instability of strained vortices," *Physics of Fluids A: Fluid Dynamics*, vol. 2, p. 76, 1990.
- [20] S. Le Dizès, "Three-dimensional instability of a multipolar vortex in a rotating flow," *Phys. Fluids*, vol. 12, pp. 2762–2774, 2000.
- [21] D. Moore and P. Saffman, "The instability of a straight vortex filament in a strain field," *Proceedings of the Royal Society of London. A. Mathematical and Physical Sciences*, vol. 346, no. 1646, p. 413, 1975.
- [22] C. Tsai and S. Widnall, "The stability of short waves on a straight vortex filament in a weak externally imposed strain field," *Journal of Fluid Mechanics*, vol. 73, no. 04, pp. 721–733, 1976.
- [23] C. Eloy, P. Le Gal, and S. Le Dizès, "Experimental study of the multipolar vortex instability," *Physical Review Letters*, vol. 85, no. 16, pp. 3400–3403, 2000.
- [24] C. Eloy and S. Le Dizès, "Stability of the Rankine vortex in a multipolar strain field," *Physics of Fluids*, vol. 13, p. 660, 2001.
- [25] C. Eloy, P. Le Gal, and S. Le Dizès, "Elliptic and triangular instabilities in rotating cylinders," *Journal of Fluid Mechanics*, vol. 476, pp. 357–388, 2003.
- [26] L. Lacaze, P. Le Gal, and S. Le Dizès, "Elliptical instability in a rotating spheroid," *Journal of Fluid Mechanics*, vol. 505, pp. 1–22, 2004.
- [27] L. Lacaze, P. Le Gal, and S. Le Dizès, "Elliptical instability of the flow in a rotating shell," *Physics of the Earth and Planetary Interiors*, vol. 151, no. 3–4, pp. 194–205, 2005.
- [28] M. Le Bars, L. Lacaze, S. Le Dizès, P. Le Gal, and M. Rieutord, "Tidal instability in stellar and planetary binary systems," *Physics of the Earth and Planetary Interiors*, vol. 178, pp. 48–55, 2010.
- [29] D. Mason and R. Kerswell, "Nonlinear evolution of the elliptical instability: an example of inertial wave breakdown," *Journal of Fluid Mechanics*, vol. 396, pp. 73–108, 1999.
- [30] R. Kerswell, "Secondary instabilities in rapidly rotating fluids: inertial wave breakdown," *Journal of Fluid Mechanics*, vol. 382, pp. 283–306, 1999.
- [31] R. Lagrange, C. Eloy, F. Nadal, and P. Meunier, "Instability of a fluid inside a precessing cylinder," *Physics of Fluids*, vol. 20, p. 081701, 2008.
- [32] R. Lagrange, P. Meunier, F. Nadal, and C. Eloy, "Precessional instability of a fluid cylinder," *Journal of Fluid Mechanics*, vol. 666, pp. 104–145, 2011.
- [33] R. Kerswell, "The instability of precessing flow," *Geophysical & Astrophysical Fluid Dynamics*, vol. 72, no. 1, pp. 107–144, 1993.
- [34] C. Wu and P. Roberts, "On a dynamo driven by topographic precession," *Geophysical & Astrophysical Fluid Dynamics*, vol. 103, no. 6, pp. 467–501, 2009.
- [35] R. Poincaré, "Sur la précession des corps déformables," *Bull. Astr.*, vol. 27, p. 321., 1910.
- [36] F. Busse, "Steady fluid flow in a precessing spheroidal shell," *Journal of Fluid Mechanics*, vol. 33, no. 04, pp. 739–751, 1968.
- [37] J. Noir, P. Cardin, D. Jault, and J. Masson, "Experimental evidence of non-linear resonance effects between retrograde precession and the tilt-over mode within a spheroid," *Geophysical Journal International*, vol. 154, no. 2, pp. 407–416, 2003.
- [38] D. Cébron, M. Le Bars, and P. Meunier, "Tilt-over mode in a precessing triaxial ellipsoid," *Physics of Fluids*, vol. 22, p. 116601, 2010.
- [39] W. Malkus, "An experimental study of global instabilities due to tidal (elliptical) distortion of a rotating elastic cylinder," *Geophys. Astrophys. Fluid Dyn.*, vol. 48, p. 123, 1989.
- [40] R. R. Kerswell and W. V. R. Malkus, "Tidal instability as the source for Io's magnetic signature," *Geophysical Research Letters*, vol. 25, no. 5, pp. 603–606, 1998.
- [41] W. Herreman, M. Le Bars, and P. Le Gal, "On the effects of an imposed magnetic field on the elliptical instability in rotating spheroids," *Phys. Fluids*, vol. 21, p. 046602, 2009.
- [42] C. Eloy, P. Le Gal, and S. Le Dizès, "Experimental study of the multipolar vortex instability," *Phys. Rev. Lett.*, vol. 85, pp. 3400–3403, 2000.
- [43] D. Cebron, M. Le Bars, J. Leontini, P. Maubert, and P. Le Gal, "A systematic numerical study of the tidal instability in a rotating triaxial ellipsoid," *Physics of the Earth and Planetary Interiors*, vol. 182, pp. 119–128, 2010.
- [44] K. Zhang, K. Chan, and X. Liao, "On fluid motion in librating ellipsoids with moderate equatorial eccentricity," *Journal of Fluid Mechanics*, vol. 673, no. 1, pp. 468–479, 2011.